Development and Testing of an Accumulation-Type Algorithm for Default and Urban Land Surfaces Using WRF Simulations

Dylan Jeffrey

A scholarly paper in partial fulfillment of the requirements for the degree of Master of Science

April 2018

Department of Atmospheric and Oceanic Science

University of Maryland

College Park, Maryland

Advisor: Dr. Daryl Kleist

Table of Contents

Abstract

The Valentine's Day Blizzard of 2007 cost 41 people their lives and over $1.3 billion in damages. New York and Vermont accrued over 30 inches of snow while Central Illinois experienced over a quarter inch of ice. Meanwhile, severe thunderstorms produced multiple tornadoes across Louisiana. Precipitation-type forecasting is exceedingly difficult to perfect. A complex winter storm with warm air aloft can produce multiple precipitation types in a small area. Steps have been made to develop algorithms to empirically predict hydrometeor phase using columnar wet-bulb temperature and fraction of frozen precipitation. However, skin temperature is also a quintessential ingredient when determining the precipitation phase that will accumulate. An alternative method is proposed allowing frozen precipitation to melt in contact with warm surfaces. A theoretical all-urban model is also discussed as a method for determining road conditions.

Acknowledgements

I would like to thank the University of Maryland Atmospheric and Oceanic Sciences Department, Dr. Tim Canty, and Dr. Daryl Kleist for their financial support throughout my time at the University. I would also like to thank Dr. Daryl Kleist for his advisement and guidance. Additionally, I would like to acknowledge Dr. Chad Kauffman, Dr. Swarndeep Gill, and Dr. Mario Majcen for their guidance and support throughout my undergraduate studies. I am thankful for my parents, Jim and Carole, for their continuous encouragement and for being my biggest fans. I also appreciate my friends who have been there for me throughout this journey. Lastly, I would like to thank my fiancée, Fatima Kizilkaya. I doubt I could have done any of this without her love and support.

List of Tables

List of Figures

List of Symbols

T_w – Wet-Bulb Temperature

T_{w_sfc} – Surface Wet-Bulb Temperature

T_{skin} – Skin Temperature

I_f – Fraction of Frozen Precipitation

SN – Snow

IP – Ice Pellets

FZRA – Freezing Rain

RA – Rain

MODIS – Moderate Resolution Imaging Spectroradiometer

WRF – Weather Research and Forecasting – Advanced Research WRF

IN – Ice Nuclei

GFS – Global Forecasting System

CMC – Canadian Modeling Center

Kts – knots

Mb – Millibar

m – Meters

°C – Degrees Celsius

Chapter 1: Literature Review

1.1 Introduction

The Valentine's Day Blizzard occurred from February 12, 2007 through February 15, 2007. On February 12, 2007, the storm developed in the Midwest and tracked through Pennsylvania and New York on February 13-14. The storm finally struck the New England states on February 14-15 (Changnon and Kunkel 2007). The National Center for Environmental Information ranked the blizzard using the Regional Snowfall Index as a Category 3 in the Northeast Region, a Category 2 in the Ohio Valley Region, and a Category 1 in the Northern Rockies and Great Plains region. This type of storm is vital to understand because it was a high impact weather event in many regions of the United States.

Illinois to Maine experienced heavy snow causing Maine and Pennsylvania to declare states of emergency. The track of the low-pressure center is shown in Figure 1 (Changnon and Kunkel 2007). Snow began in Illinois in the evening hours of February 12, confirmed through METAR observations. The National Weather Service reports that areas of southern Illinois received a quarter inch of ice followed by 2-4 inches of ice pellets. Springfield, Illinois experienced 11.2 inches of snowfall in a 24-hour period. Areas of New York and Pennsylvania received over 20 inches of snow with some areas

Figure 1: *Illustration of the Valentine's Day Blizzard central low-pressure track. (Changnon and Kunkel 2007)*

accruing over one inch of ice pellets. The storm also caused severe thunderstorms with multiple tornadoes across the southern portion of the country.

Two experiments will be discussed in this article. The first experiment will be to develop an accumulation-type algorithm based off the precipitation-type algorithms from Ramer (1993) and with modifications by Pytlak et al. (2010) and Bourgouin (2000). The accumulation-type algorithm will allow for hydrometeors to change phase as it encounters the ground. This is intuitive as snow and ice cannot accrue on surfaces above freezing. The atmosphere must cool the land surface through sensible heat and latent heat to temperatures below 0°C to allow for frozen precipitation to accumulate. Preliminary testing will be performed using the case study and MODIS 21-category land use indices for a difference in precipitation-type and accumulation-type. The second experiment will act as a test for the applicability of the accumulation-type algorithm for transportation purposes. Using the Weather and Research Forecasting - Advanced Research WRF model (WRF), the domain's land surface will be altered to the MODIS urban category during the preprocessing system. The model output will be compared to the original precipitation-type algorithm and the accumulation-type algorithm on the urban model.

1.2 Winter Precipitation

Frozen hydrometeors are formed through ice nucleation. Two processes can cause ice nucleation: homogenous nucleation and heterogenous nucleation. Homogenous nucleation occurs when frozen precipitation forms without the presence of a nuclei. According to Rogers and Yau (1989), this requires an arbitrarily high level of

supersaturation and supercooling that are not typically observable in the atmosphere. Thus, homogenous nucleation is not naturally observable.

Frozen precipitation is typically initiated through heterogenous nucleation. This occurs when a hydrometeor is formed in the presence of an Ice Nuclei (IN) which are scarce compared to cloud condensation nuclei (CCN) (Murray et al. 2012). Rogers and Yau (1989) describe four main methods for heterogeneous nucleation as heterogeneous deposition, condensation and then freezing, contact nucleation, and immersion. Heterogeneous deposition occurs when a vapor molecule changes phase directly to an ice crystal. Condensation and then freezing happens when an IN forces supercooled water to condense around it and then freezes over time. Contact nucleation occurs when an IN encounters a water droplet and causes it to freeze. Immersion arises when an IN enters a supercooled droplet and serves as the nucleus that a liquid water droplet can freeze around. IN concentrations increase by a factor of ten for every 4°C cooling.

The main growth mechanism of a frozen hydrometeor is the Bergeron process which transpires when ice crystals come in contact with supercooled water within a mixed-phase cloud (Murray et al. 2012, Rogers and Yau 1989, Korolev 2007). The Bergeron process grows ice particles due to a lower vapor pressure between surrounding ice crystals and supercooled water droplets. This causes ice crystals to thrive at the expense of water droplets, allowing clouds to contain large ice crystals with low concentrations (Murray et al 2012). Korolev (2007) also mentions two other processes that may inhibit the Bergeron process: simultaneous growth or evaporation of liquid droplets and ice particles. Liquid droplets may compete for the water vapor which

will slow the depositional growth. This is most common during entrainment. Water droplets and ice crystals may also evaporate or sublimate, respectively. It is important to consider the vapor pressure of the cloud, liquid water, and ice crystals within a mixed-phase cloud to determine which growth mechanism is favored (Korolev 2007).

During winter storms, accurate precipitation-type forecasting is crucial when preparing for the event (Elmore et al. 2015). Many storms consist of a precipitation-type transition zone. In fact, Moyer (2000) performed a climatological survey and discovered that the Greenville-Spartanburg airport in South Carolina received at least two precipitation-types in 80-90% of winter storms. Algorithms for precipitation-type forecasting are reliable at differentiating between rain (RA) and snow (SN) as model uncertainty has little impact on the distinction. In contrast, ice pellets (IP) and freezing rain (FZRA) are much more difficult to predict (Reeves et al. 2014). IP and FZRA thermal structures are too similar and a minor model bias will frequently cause an error in the forecast (Reeves et al. 2014). Precipitation-type is critically dependent upon the columnar temperature distribution and the intensity of the melting and refreezing layer (Zerr 1997). Stewart and King (1986) defines mixed precipitation as SN, IP, and FZRA occurring simultaneously. The typical cause for mixed precipitation is a variation in hydrometeor size. Large snowflakes may not melt in a weak melting layer while small snowflakes could transition completely to liquid (Stewart and King 1986; Zerr 1997). As thermal profiles fluctuate within several degrees of 0°C in the lower troposphere, frequent precipitation-type changes may occur, and latent heat impacts will alter the thermal profile accordingly (Lackmann et al. 2002).

Although the latent heat effects of melting and freezing are weak compared to the effects of evaporation and condensation, local changes to the thermal profile can occur due to the phase change as snow falls through a low-level, warm layer and converts to FZRA or IP. To maintain FZRA and IP precipitation-types, the warming from advection must surpass the impacts of latent cooling (Lackmann et al. 2002). A forecaster generally uses atmospheric values like 1000-500 mb thickness to determine the precipitation-type where values of less than 5400 meters is considered the quintessential ingredient for frozen precipitation. However, Heppner (1992) suggests this does not resolve lower atmospheric warm layers. To delineate from snow and rain, an 850-700 mb thickness threshold of 1550 m is used. Thickness values greater (less) than 1550 m are RA (SN).

A melting layer will act to change the hydrometeor to a liquid when a low-level warm air intrusion is present. If the air below the warm layer is less than 0°C, supercooling or freezing will take place leading to IP or FZRA precipitation (Lackmann et al 2002). Even a slight model bias in temperature can cause mis-classification. Empirical algorithms have been developed to aid in determining the hydrometeor-type during winter storms (Reeves et al 2014).

1.3 Precipitation-Type Algorithms

Ramer (1993) uses columnar wet-bulb temperature (T_w) and fraction of frozen precipitation (I_f) to determine hydrometeor type. A top-down method is used to trace hydrometeors from precipitation-generation to the surface. Statistical methods were used to develop thresholds for the generating layer's T_w, surface T_w (T_{w_sfc}), profile T_w, and surface I_f to place precipitation into categories of SN, FZRA, IP, RA, or mixed. The

first decision is to deduce if $T_{w\_sfc} \geq 2°C$. If so, the model predicts RA. In the alternative, the model filters through the profile T_w for values exceeding 0°C to determine if a melting layer is present. If a melting layer is not present, SN is predicted. When a melting layer is present, the model searches for the generating layer to determine if ice is present. The generating layer is defined as the first region below 400 mb with RH > 90% for at least 16 mb. Without ice in the column, the model limits the precipitation-type to RA and FZRA. Otherwise, the model analyzes I_f. High values of I_f allow for hydrometeors to refreeze while low values restrict freezing. The final decision is if T_{w_sfc} > 0°C or < 0°C. The former condition will classify as RA or FZRA while the latter will classify as mix or freezing mix. The Ice Accretion Forecasting System (IAFS) uses a variation of this algorithm for the model's precipitation-type classification (Pytlak et al. 2010).

Baldwin et al. (1994) uses derived numerical model data and observed sounding data in case studies to empirically categorize precipitation-type. The algorithm works on a series of "Yes" or "No" decisions. If the model predicts a coldest saturated level greater than 269 K, then the decision is dependent on the lowest layer temperature due to the presence of ice crystals. A lowest layer temperature of less than 273 K results in FZRA while the contrary predicts RA. The Baldwin algorithm utilizes an above-freezing area to predict the chance of melting. If the area of T_w > 273 K is less than 350 K m, melting is not achievable, and snow is predicted. In the opposite scenario, melting can be achieved and is now evaluated for the odds of refreezing. If the area of below freezing T_w in the lowest 150 mb is less than -2500 K m and the lowest-level T_w above freezing is less than 350 K m, then refreezing is assumed and IP is predicted.

Otherwise, the precipitation is in liquid phase as it hits the surface. If $T_{w\_sfc} \leq 0°C$, FZRA is predicted. To the contrary, a $T_{w\_sfc} > 0°C$ will be rain. This algorithm was implemented into the Eta model in January 1994 (Black 1994).

The Bourgouin (2000) algorithm utilizes statistical analyses of 173 soundings to discriminate the typical thermal profiles for precipitation-types. RA is forecasted if the thermal profile has only one crossing of the 273 K isotherm with sufficient depth aloft. Snow is forecasted when no melting layer exists. Most algorithms use T_w where the Bourgouin algorithm utilizes temperature (T). Also atypical to other algorithms, hydrometeor-type is assumed to be frozen upon generation. This algorithm was implemented into the Canadian Modeling Center (CMC) models in spring 1995.

1.4 Urban Environments Impacts on Winter Precipitation

Precipitation-type is also dependent on T_w when determining the impacts of winter weather on society. Accumulation of snow and ice on roads substantially increases the risk of weather-related incidents. Knollhoff et al (1998) found that urban road temperatures were 2 to 5°F (1 to 3°F) higher than rural roadway temperatures during clear skies (cloudy skies). The dissimilarities between urban and rural conditions greatly depend on radiative fluxes (Landsberg 1981). Changnon (2003) found that New York, Chicago, St. Louis, and Washington, D.C. all showed distinguishable decreases in FZRA events due to the urban heat island effect. Modeling can be performed on road temperatures to assist winter maintenance operations on what action should be taken in maintaining safe road conditions (Sherif and Hassan 2004). Without below freezing surface temperatures, precipitation will melt on contact with the surface excluding scenarios when accumulation rates exceed melt rates (Sherif and Hassan 2004).

Additionally, hoar-frost may be deposited on roads when dew point temperatures exceed asphalt temperatures. Hoar-frost can be predicted using air temperature, wind speed at 5 m, and road surface temperature (Karlsson 2001). Pavement temperatures are vital in properly forecasting weather-related hazards on transportation (Sherif and Hassan 2004, Knollhoff et al 1998, Karlsson 2001)

1.5 Synoptic Overview

A synoptic discussion is presented using Global Forecasting System (GFS) reanalysis data (NCEP 2000) for the Valentine's Day Blizzard. Figure 2A-F show 300 mb winds (kts). Shaded fill are local maxima wind speeds exceeding 40 kts for February 12 at 12z through February 15 at 00z in 12 hours increments, respectively. Winds at 300 mb are relatively weak for most of the storm. A weakly amplified shortwave in the 300 mb wind pattern exists over the four corner states during storm initiation. Aside from this, little driving forces exist in the upper levels, as the subtropical and polar jet are weak until after the storm passes. On February 14 at 12Z, the subtropical jet acts to push the storm off the east coast. Overall, the 300 mb winds had little influence on the intensity of the storm and amplification was likely driven by low-to-mid- level phenomena.

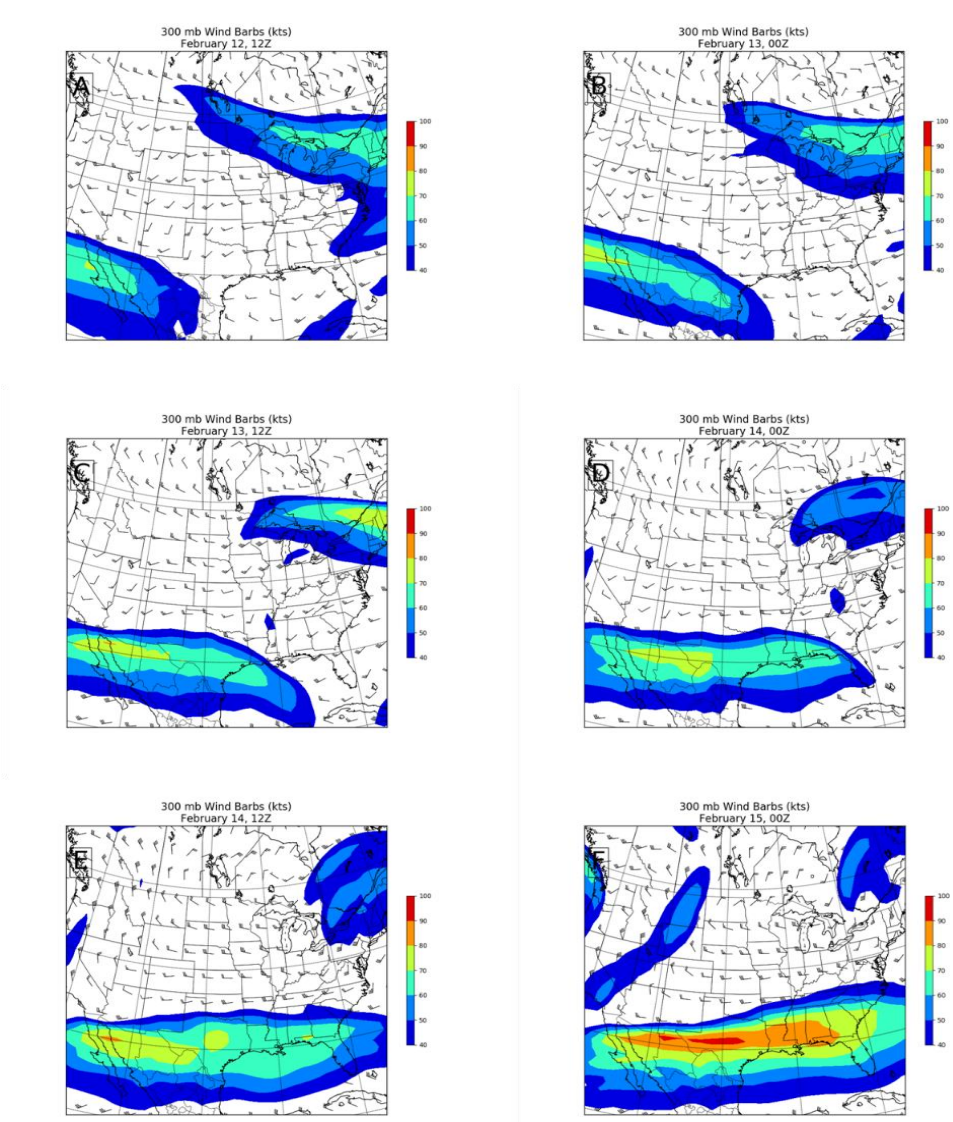

Figure 2A – F: 300 mb wind barbs and jet streaks for February 12 at 12z - February 15 at 00z derived from GFS 1° Reanalysis data. Winds are relatively weak and zonal across much of the Midwest and during the storm. The storm has little driving forces at the 300 mb level.

Figure 3A-F show 500 mb geopotential heights (m), wind barbs (kts), relative humidity (%) and temperatures (°C) for February 12 at 12z through February 15 at 00z in 12 hour increments, respectively. The storm is well supported by the 500 mb set-up. High moisture and cold temperatures would provide an abundance of ice crystals to the lower portion of the storm. In Figure 3A, a strong baroclinic zone exists across the four-corner states. This is critical for the development of the storm as the baroclinic zone is

influenced by the shortwave present at both 300 mb and 500 mb. On February 14 at 00z (Figure 3D), the 500 mb trough becomes negatively tilted. In Figure 3E, the storm begins to move off the coast despite the presence of the 500 mb shortwave. In Figure 3F, the shortwave continues northeast, steering around the 500 mb cut off low over Canada.

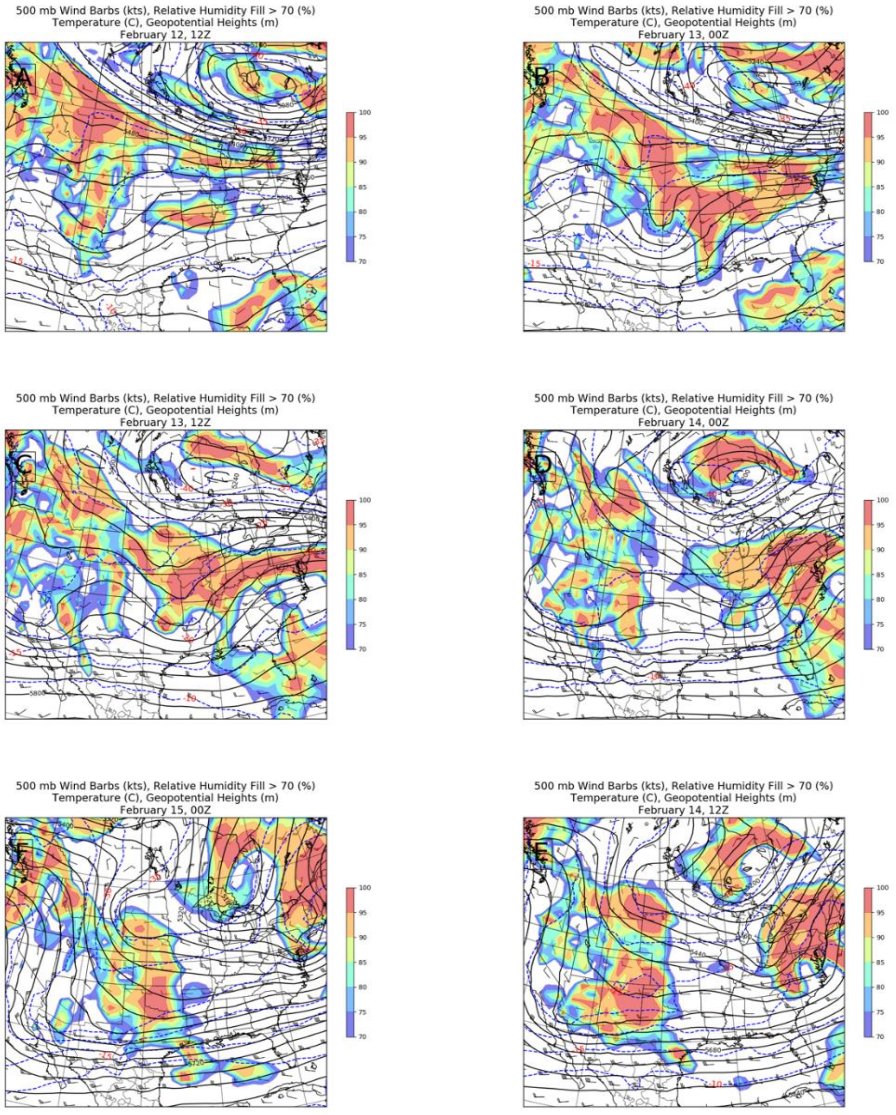

*Figure 3a – f show the 500 mb wind barbs (kts), relative humidity > 70 (%), temperature (°C), and geopotential heights (m) for February 12 at 12z – February 15 at 00z derived from GFS 1° Reanalysis data. The amplified trough in heights in **b** deepen the storm and drive much of the vertical motion through vorticity. In addition to the vorticity, a baroclinic zone existed that drove additional instability. Relative humidity values are typically above 90% for the bulk of the storm, hinting that the generation layer is relatively high and below freezing. This should allow for ice nuclei throughout the storm.*

Figure 4A – F show 850 mb wind barbs (kts), skin temperature contours (°C), and maximum temperatures in the 1000 – 750 mb column for February 12 at 12z through February 15 at 00z in 12 hour increments, respectively. The green shaded regions indicate an area with a melting layer and subfreezing skin temperatures. This area is conducive for FZRA or IP precipitation. The green shaded region is obvious at the beginning of the storm and persists during the 00z hours but deteriorates during the 12z plots. The sustainability of the melting layer is likely driven from strong, warm air advection which exceeds the rate of latent cooling. The unique conditions at the 850 mb level trigger most of the complex winter precipitation.

While the storm's upper level structure was not impressive, high columnar moisture and veering winds allowed for persistent icing and snow accumulations from February 12 to February 15. Changnon and Kunkel (2007) reported 41 deaths and $1.373 billion in damages, mostly due to icing and snow accumulation. The primary focus of this research will be to diagnose the phase in which the precipitation accumulated.

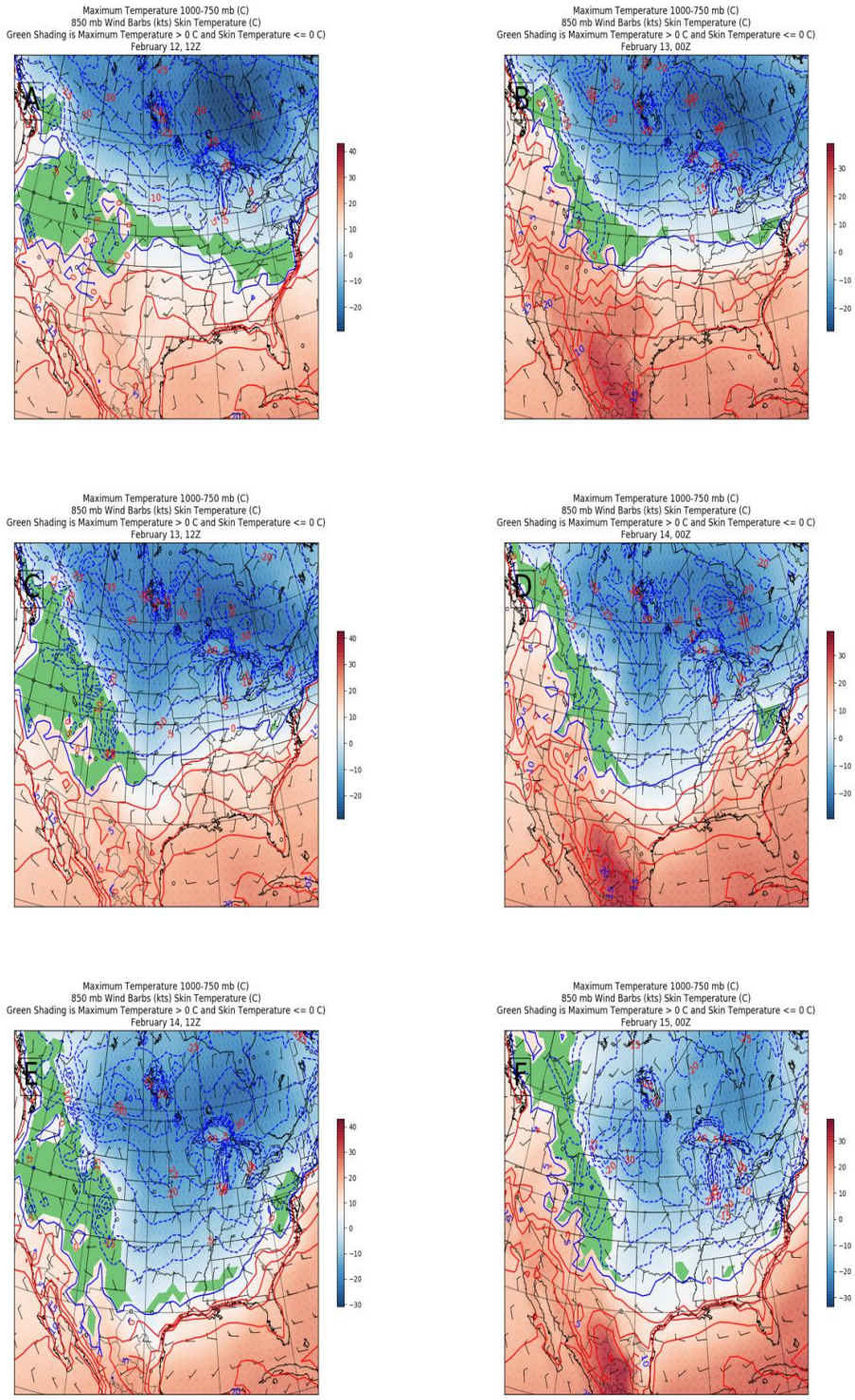

*Figure 4a – f show the 850 mb wind barbs (kts), skin temperature (°C), and maximum temperature in the 1000 – 750 mb column (°C) for February 12 at 12z – February 15 at 00z derived from GFS 1° Reanalysis data. The green shading indicates a region with a melting layer and skin temperatures below freezing. In **A**, during storm initiation, the conditions are conducive for mixed precipitation across the Midwest. Strong southerly flow brings warm, moist air in the lower atmosphere. This will act to sustain the melting layer during daylight hours amidst vast latent cooling.*

Chapter 2: Data and Methodology

2.1 Data and Model

The WRF initial and boundary conditions are driven by 1° GFS reanalysis data (NCEP 2000). Land surface category data are derived from MODIS for the first experiment, to be discussed in the next section. Sensitivity tests were performed for seven different combinations of schemes and were qualitatively assessed with careful consideration to precipitation and skin temperature (T_{skin}). While most variables had little variation from each other, significant variation existed with T_{skin} particularly after the urban land surface was considered. For this purpose, the chosen scheme was based off which combination provided the most realistic representation of T_{skin}. The parameterizations chosen are shown in Table 2. The land surface scheme was chosen carefully and is important to note. The Noah-LSM produced T_{skin} values exceeding 40°C while Noah-MP produced reasonable T_{skin} values. Noah-MP also maintained reasonable outputs after the surface is parameterized to all urban land-type.

Scheme	MP	PBL	Cumulus	Land Surface	UA_Snow_Phys
Options	Thompson	MYJ	Kain-Fritsch	Noah-MP	True

Table 1: The WRF model physics options used for this study. For more information, see: http://www2.mmm.ucar.edu/wrf/users/phys_references.html

The domain for the experiment is shown in Figure 5. Spatial and temporal resolution are 3-km and 3-hr, respectively. The model is initiated on February 11 at 00z and run until February 15 at 00z. The storm does not begin to impact the studied

domain until 36 hours beyond the model initialization to allow for T_{skin} of the default run and T_{skin} of the urban run to diverge independent of the initial conditions.

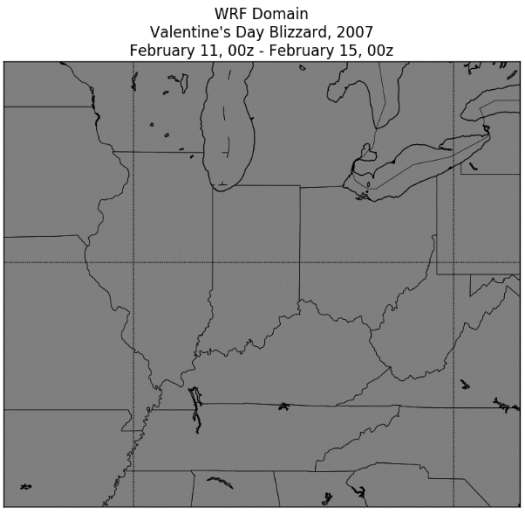

Figure 5: Domain used for the WRF Model runs.

2.2 Methodology

2.2.1 Experiment 1

The purpose of this research is to develop and test an accumulation-type algorithm. The accumulation-type is defined as the precipitation-type that will accrue on the land surface. The first step in determining the accumulation-type is to derive the hydrometeor-type. The Ramer algorithm was determined to be statistically the best algorithm and will be used as a starting point (Musilek et al. 2009). Pytlak et al. (2010) uses a modified Ramer algorithm with some success in optimizing an ice accretion forecasting system. This research will use the modified algorithm from Pytlak et al. (2010) with the assumption from Bourgouin (2000) that all hydrometeors begin as frozen which is a reasonable assumption based on the relative humidity and temperature values at 500 mb (Figure 3).

Figure 6 shows the decision tree for precipitation-type used as the control for this study. The first step in precipitation-type discrimination is analyzing T_{w_sfc}. Since T_w is not provided by the default WRF output, the wrf-python (Ladwig 2017) module is used to calculate T_w for values of relative humidity (RH) less than 100%. Otherwise, $T_w = T$. If $T_{w\_sfc} < -6.6°C$ or $T_{w\_sfc} > 2°C$, SN or RA are defined respectively. If the T_{w_sfc} lies

between these two values (-6.6°C < T_{w_sfc} < 2°C), the profile T_w must be investigated. If a melting layer in the T_w profile does not exist, then the hydrometeor is defined as snow. If a point on the T_w profile is partially above 0°C, then the I_f is investigated. An I_f = 1 results in SN while 1 > I_f ≥ 0.85 results in IP. However, I_f < 0.85 require further investigation to discriminate from IP, FZRA, or RA. T_{w_sfc} is revisited. An I_f ≤ 0.04 and a T_{w_sfc} > 0°C (T_{w_sfc} ≤ 0°C) will be diagnosed as RA (FZRA). Likewise, if 0.85 > I_f > 0.04 and T_w is > (≤) 0°C, then FZRA (IP) is defined.

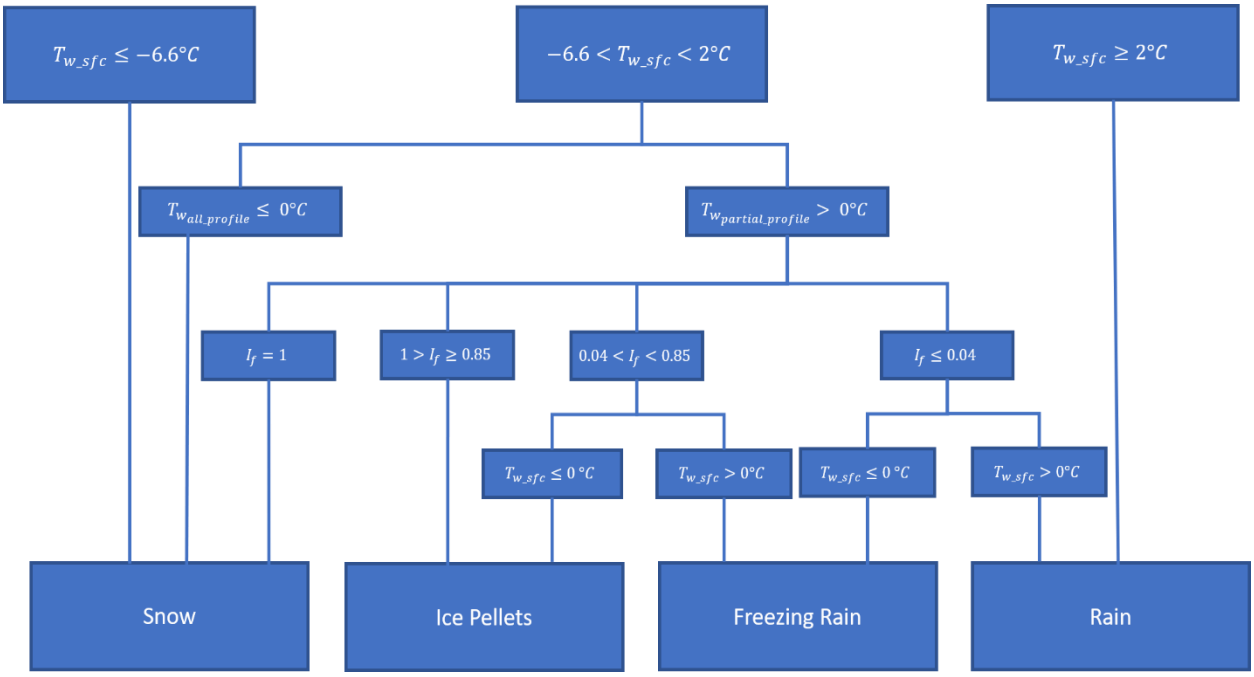

Figure 6: Precipitation-type decision-tree derived from Ramer (1993), Pytlak et al. (2010), and Bourgouin (2000).

The accumulation-type algorithm considers the precipitation-type to also be a function of T_{skin} and is shown in Figure 7. The accumulation-type algorithm assumes liquid (frozen) precipitation freezes (melts) on contact when T_{skin} ≤ 0°C (T_{skin} > *0*°C). This is a safe assumption as long the accumulation rate does not exceed the melt rate, which only occurs in extreme conditions. RA can only accumulate when T_{skin} > 0°C. When T_{skin} ≤ 0°C, a similar decision tree to Figure 6 is considered. Another difference is when all of the following decisions are made: an Intermediate T_{w_sfc}, a partial-columnar

T_w > 0°C, and I_f ≤ 0.04. Under the assumption that liquid precipitation will always cool and freeze on contact with sub-freezing T_{skin}, this condition will produce FZRA.

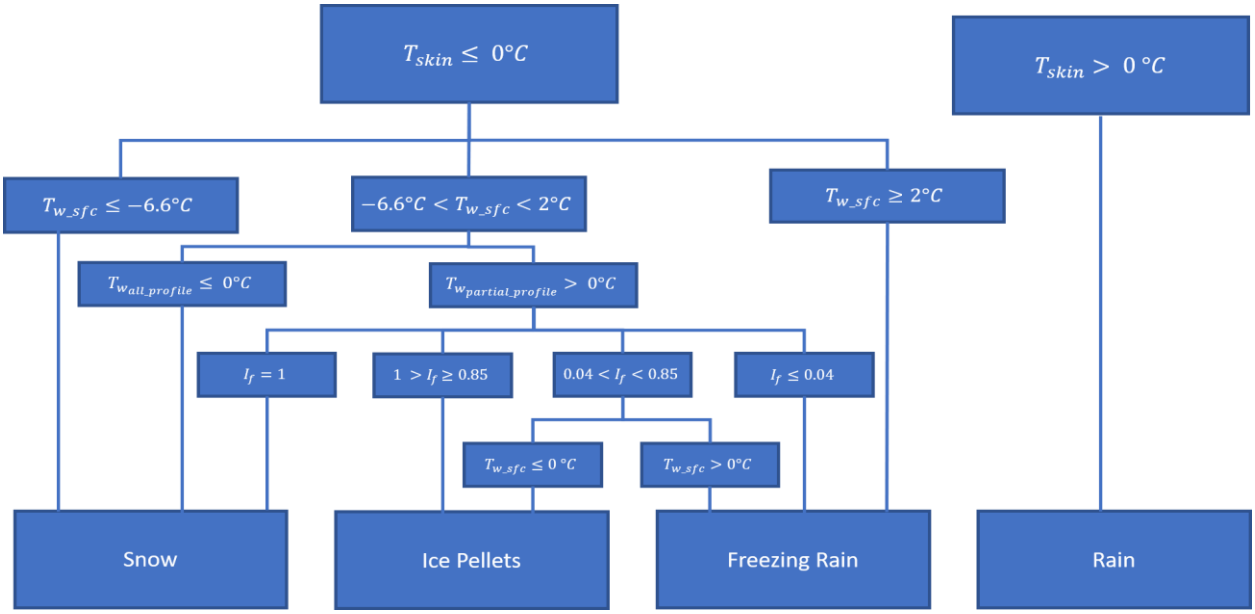

Figure 7: Accumulation-Type decision-tree. Similar to the precipitation-type (Figure 6) except with a dependence on T_{skin}*. The skin temperature must reduce to below-freezing before FZRA, IP, or SN can accumulate.*

The accumulation-type algorithm will be analyzed using WRF output from the Valentine's Day Blizzard and compared to the modified Ramer algorithm. Both the accumulation-type and precipitation-type algorithm are analyzed using the same WRF model output. The decision trees are calculated using Python and plotted across the WRF domain. The two algorithms are contrasted to determine how the precipitation-type might change as it comes in contact with the surface. The hypothesis is that the accumulation-type should differ from the precipitation-type when T_{skin} is warmer than 0°C, independent of the hydrometeor-type.

2.2.2 Experiment 2

The purpose of the second experiment is to determine how successfully the algorithm determines road conditions during winter storms. The WRF Preprocessing System (WPS) is shown in Figure 8 from the WRF user's manual. Geogrid constructs

the domain and assigns the land surface. In the case of the first experiment, MODIS 21-category land use indices are used. The default land use indices are shown in Figure 9. The entire domain is altered to all urban/built up using the Geogrid output files and Python. The table category, decoded category, albedo, soil moisture, surface emissivity, roughness length, and surface heat capacity for the three most prominent categories and the urban/built-up are shown in Table 1.

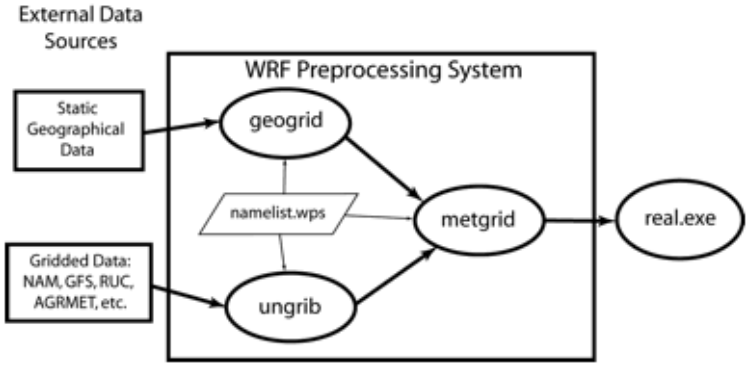

Figure 8: WRF Preprocessing System. Before metgrid is run, the output of geogrid is edited to all urban land surface for experiment 2.

Following the process of editing the geogrid files, the WRF model is run using identical physics schemes to the default run (Table 1). Since the accumulation-type algorithm only differs from the precipitation-type algorithm by its variance in T_{skin}, the main objective of experiment 2 is in the difference between default T_{skin} and urban T_{skin}. A qualitative analysis is done to analyze how the urban land surface heats and cools versus the default land surface. After this is

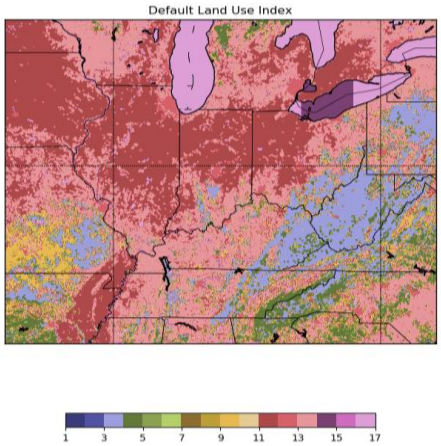

Figure 9: Default land use index from MODIS used for the default model run. The primary land types are Croplands, Natural Mosaic, and Deciduous forest

Table Category	Decoded	Albedo	Soil Moisture	Sfc Emissivity	Roughness Length	Sfc Heat Capacity
12	Croplands	17	0.30	0.985	15	$25 * 10^5 Jm^{-3}K^{-1}$
14	Natural mosaic	18	0.25	0.98	14	$25 * 10^5 Jm^{-3}K^{-1}$
4	Deciduous Broadleaf Forest	16	0.30	0.93	50	$25 * 10^5 Jm^{-3}K^{-1}$
13	Urban/ Built-Up	15	0.1	0.88	80	$18.9 * 10^5 Jm^{-3}K^{-1}$

Table 2: Values for the land surface of the three most prominent land types in the default model (blue) and values for the land surface for the urban model (red)

performed, the precipitation-type algorithm and the accumulation-type algorithm are analyzed on the urban land surface. The plots use the thermal and precipitation data from the default land surface model run for the urban accumulation-type plots. This is done to avoid slight differences that the urban land surface may have caused to other parameters than T_{skin}. The accumulation-type will likely have a more robust area of RA at the expense of IP and FZRA due to a lower specific heat.

Chapter 3: Analysis and Discussion

3.1 Experiment 1 Analysis

Experiment 1 develops an algorithm that predicts the precipitation-type that will accumulate when a hydrometeor lands on the surface. The results of the accumulation-type algorithm is compared to that of the precipitation-type algorithm using WRF and the Valentine's Day Blizzard on the default land surface. The analysis will be done qualitatively for maximum daytime heating at 21z and maximum nighttime cooling at 09z for February 12 – February 14. The purpose for this is that the accumulation-type

should have the strongest contrast from the precipitation-type at 21z and the strongest comparison at 09z. The following figures show the predicted precipitation-type on the left and the predicted accumulation-type on the right. RA is colored red, FZRA is colored pink, IP is colored light blue, and SN is colored dark blue.

Figure 10 displays a strength of the accumulation-type algorithm. At storm onset, skin temperatures did not cool as rapidly as the air. The columnar thermal conditions were conducive for FZRA and IP in central Missouri and the mountains of West Virginia. However, the accumulation-type is RA. As seen from Figure 10B, the skin temperature is above freezing; frozen hydrometeors will likely melt upon impact.

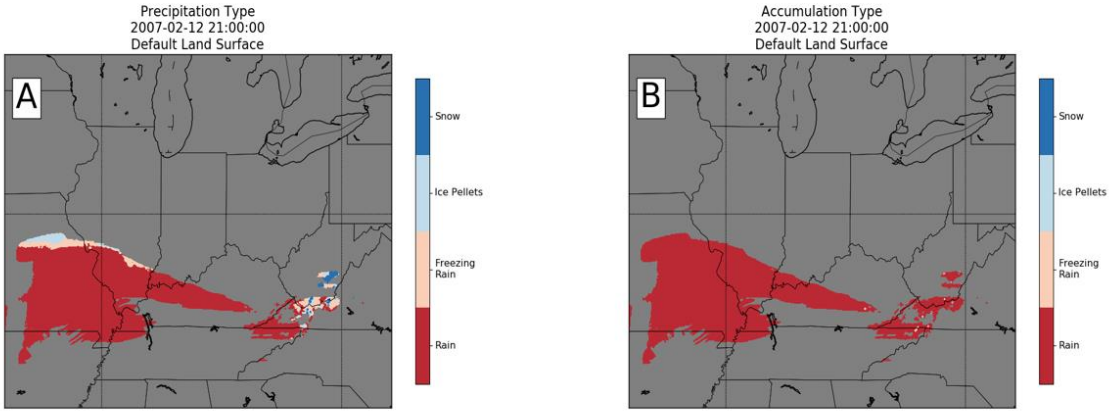

Figure 10A-B: Figure A represents the precipitation-type on the default land surface and acts as the control run for this experiment. Figure B represents the accumulation-type on the default land surface. Notice how Figure A shows some frozen precipitation, but T_{skin} *is above freezing and all hydrometeors would turn to liquid on contact with the surface.*

Upon nightfall on February 13 at 09z (Figure 11), the land surface rapidly cools and is in close equilibrium to the air temperature. Figures 11A and B are nearly identical with a slight exception in southwestern Illinois. Frozen hydrometeors will readily accumulate in regions north of the RA line. In Lake Michigan on Figure 11B, rain is suspected to accumulate. This is due to lake waters that are also above freezing.

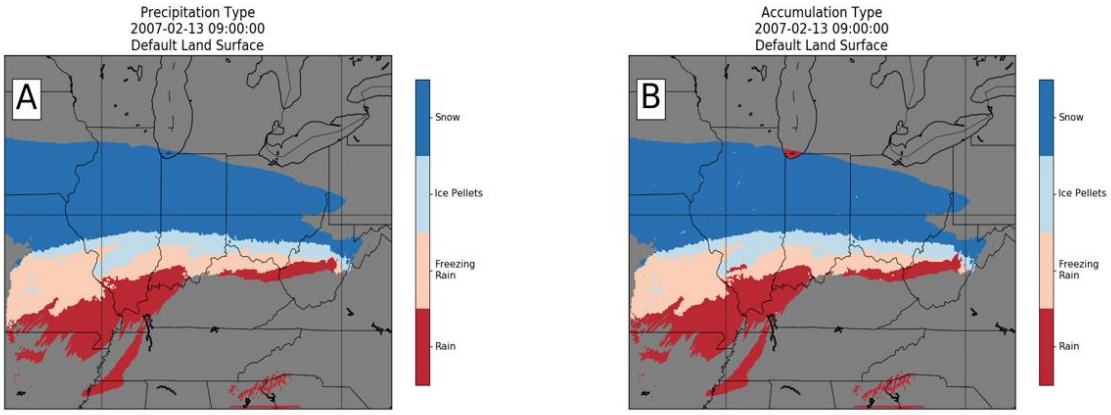

Figure 11A-B: Figure A represents the precipitation-type on the default land surface. Figure B represents the accumulation-type on the default land surface. T_{skin} *decreased overnight and most of the precipitation is accumulating.*

The next afternoon on February 13 at 21z (Figure 12), the land surface heats due to radiational effects. The RA-FZRA line moves slightly north in Figure 12B compared to Figure 12A. In Virginia, there is also a slightly broader region of RA accumulation where frozen precipitation may melt in contact with the surface.

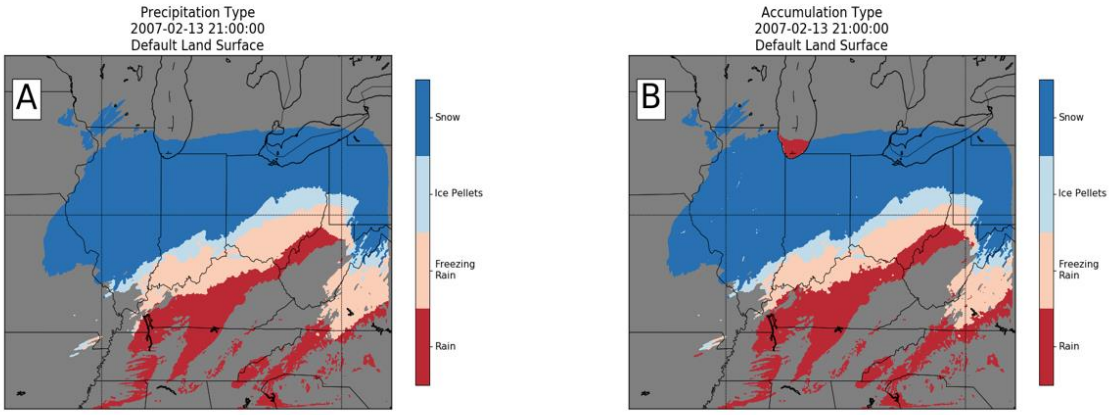

Figure 12A-B: Figure A represents the precipitation-type on the default land surface. Figure B represents the accumulation-type on the default land surface. Portions of northern Kentucky have precipitation melting at the surface, but the figures look very similar

Similar to the previous night, the land surface releases heat to the air and cools to equilibrium on February 14 at 09z (Figure 13). The accumulation-type and the precipitation-type do not show much of a difference, as T_{skin} is below freezing for most of the frozen precipitation region. The following afternoon on February 14 at 21Z (Figure 14) shows the storm as it passes on into New York. The land surface had cooled for the entirety of the storm and is accumulating SN.

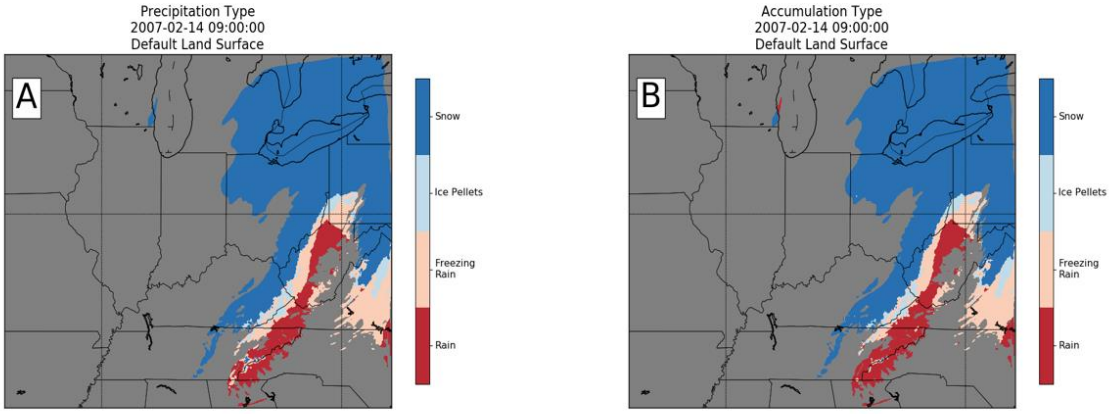

Figure 13A-B: Figure A represents the precipitation-type on the default land surface. Figure B represents the accumulation-type on the default land surface. The accumulation-type is equivalent to the precipitation-type

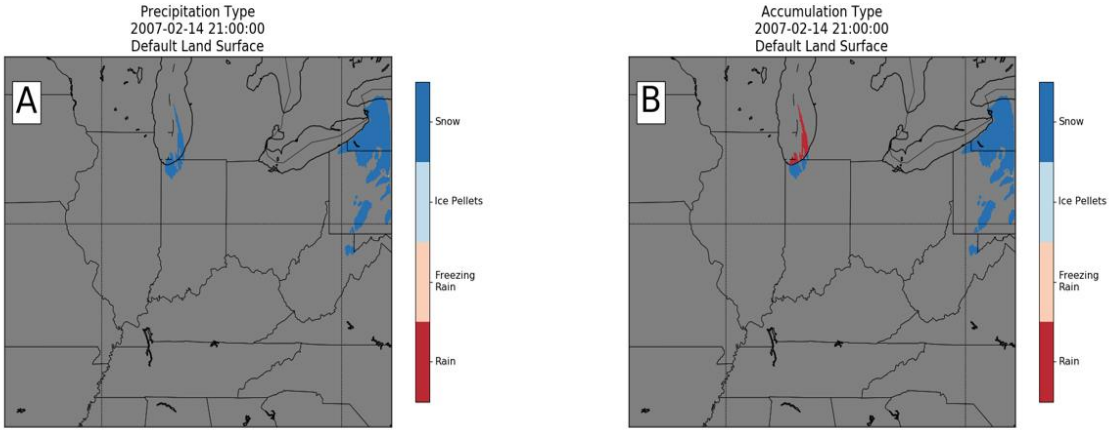

Figure 14A-B: Figure A represents the precipitation-type on the default land surface. Figure B represents the accumulation-type on the default land surface. The storm has transitioned completely to snow and moved to the northeast.

3.2 Experiment 1 Discussion

When considering the accumulation-type, the precipitation-type is useful for the bulk of the storm. This does not hold true for all time periods. When warm air precedes a winter event, the land may heat up significantly. As a storm passes, frozen precipitation may occur for hours before cooling the land surface to below-freezing. Once T_{skin} reduces to below freezing, it is reluctant to heat back to above freezing. Much of this cooling happens at night. When considering the impacts of winter precipitation, especially within the precipitation transition zone, the accumulation-type algorithm is most useful near storm-onset. However, the default land surface does not give the most appropriate representation of the impacts to transportation. For this, Experiment 2 is performed.

3.3 Experiment 2 Analysis

Experiment 2 is similar to Experiment 1 in that the goal is to compare the precipitation-type algorithm to the accumulation-type algorithm. The nuanced difference is the altering of the land surface to an entire urban region. This provides some limitations as this methodology does not allow for small-scale cooling due to local vegetation, like a grass-covered median's influence on highway temperature. The first step is to evaluate T_{skin} for the default land surface and the urban land surface. The main thermodynamic changes on T_{skin} are derived from the change in heat capacity as seen in Table 2. The urban/built-up land surface has a heat capacity of $18.9 * 10^5\ Jm^{-3}K^{-1}$ while most of the default land surface has a heat capacity of $25 * 10^5\ Jm^{-3}K^{-1}$. This means that the urban/built-up land surface should change temperature more readily than the default land surface. The first step to evaluate the

accumulation-type will be to investigate how T_{skin} differs between the urban land surface and the default land surface. The following figures show the difference between the urban T_{skin} and the default T_{skin}. Red colors indicate when the urban land surface is warmer than the default land surface for the same time step.

3.3.1 Skin Temperature

Figure 15 is the difference between the initial temperatures for the model run. This is a limitation to this methodology as the initial temperatures would typically be different. Since these temperatures are identical, the model is initiated before the storm to allow for T_{skin} to heat up independent of initial conditions, before storm initiation.

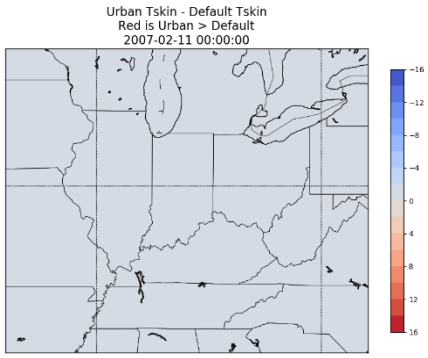

Figure 15: Difference in T_{skin} between the initial temperature of the urban run and default run. Notice this is zero because the initial conditions are the same for both model runs.

Figure 16 shows the difference in T_{skin} on February 12 at 21Z. This is when heavy precipitation began to fall. The southern portion of the domain in the urban run is uniformly warmer than the default run while the central CONUS consists of similar temperatures in both model runs. This correlates well with the snow cover for the same period (Figure 17). When the default

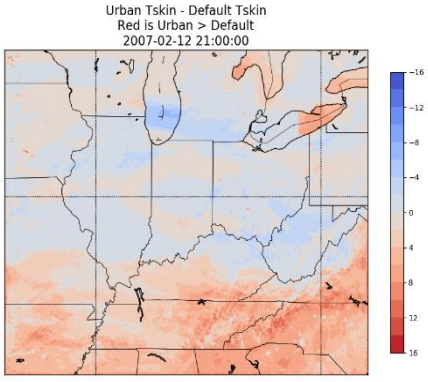

Figure 16: Difference in T_{skin} between of the urban run and default run.

model begins to accumulate SN but the urban model does not, T_{skin} will increase far more in the urban model than the default model.

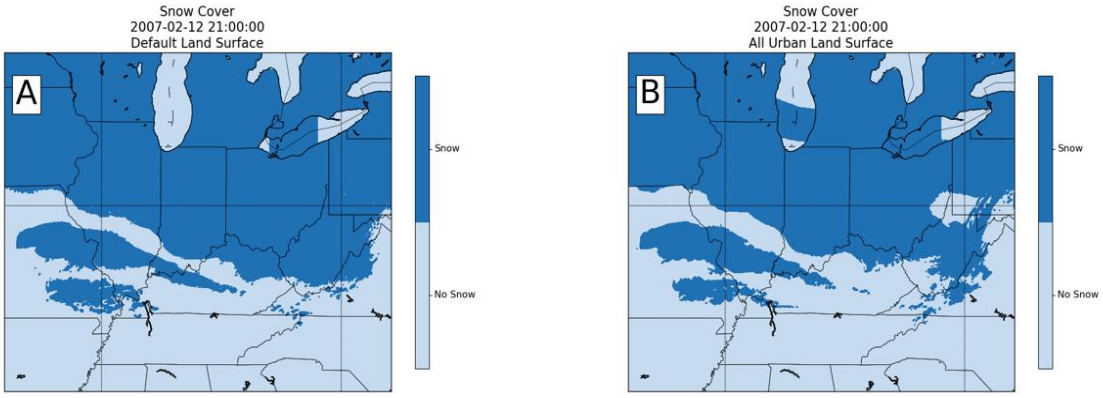

Figure 17A-B: Figure A shows the snow cover of the default model and Figure B shows the snow cover of the urban model at February 12 at 21Z. Notice the areas with snow cover have similar T_{skin} while the urban model skin is warmer in areas without snow cover

Figure 18 shows the difference in T_{skin} on February 13 at 09Z. At night, the differences in temperatures become less polarizing. SN is expected to continue to accumulate in both models where both skin temperatures are similar.

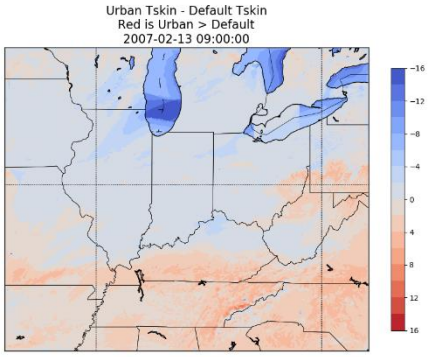

Figure 18: Difference in T_{skin} between of the urban run and default run.

The following afternoon on February 13 at 21Z (Figure 19), temperatures over northern Arkansas and western Texas increased exponentially compared to the default land surface. In the area where frozen precipitation fell, the difference is

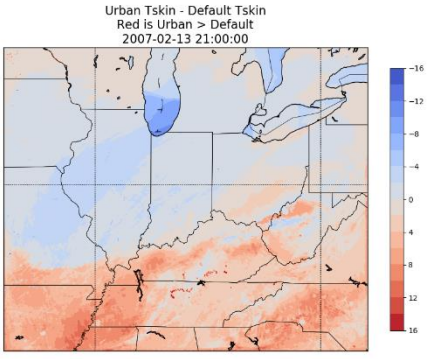

Figure 19: Difference in T_{skin} between of the urban run and default run.

minimal. In the southwestern portion of the domain, T_{skin} in the urban model is up to 12°C warmer than the default model.

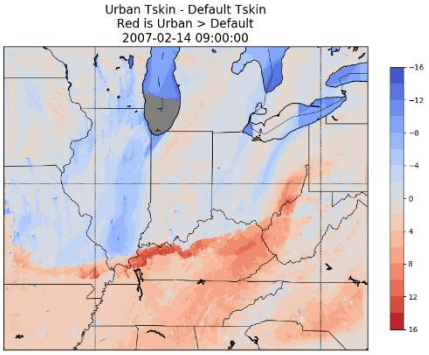

Figure 20: Difference in T_{skin} between of the urban run and default run

At nighttime on February 14 at 09Z (Figure 20), and the following afternoon (Figure 21), a robust boundary forms along northwestern Kentucky. Temperatures in the urban model run have risen exponentially beyond the temperatures of the default run while north of this line, the temperatures continue to be similar.

The hypothesis for this robust boundary in urban and default temperatures in the southern portion of the domain is frozen precipitation cover. The region in which SN, IP, or FZRA accumulated would have a different surface temperature than areas without any frozen accumulation. The next step in Experiment 2 is to determine how these changes in temperatures may change how a hydrometeor accumulates on an urban land-type compared to the precipitation-type.

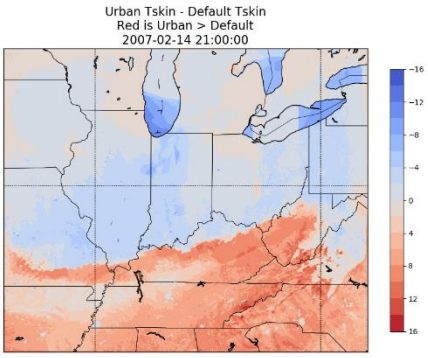

Figure 21: Difference in T_{skin} between of the urban run and default run

3.3.2 Accumulation-Type

This section presents precipitation-type (A) and accumulation-type (B) for the default land surface and urban land surface. Regions where T_{skin} are above-freezing are limited to rain, while regions with T_{skin} below-freezing allow for the frozen precipitation-type in (A) to accumulate. Figure 22

represents the beginning of frozen precipitation. The temperatures in the urban land surface are all above freezing and all the frozen accumulation is sure to melt at 21Z on February 12.

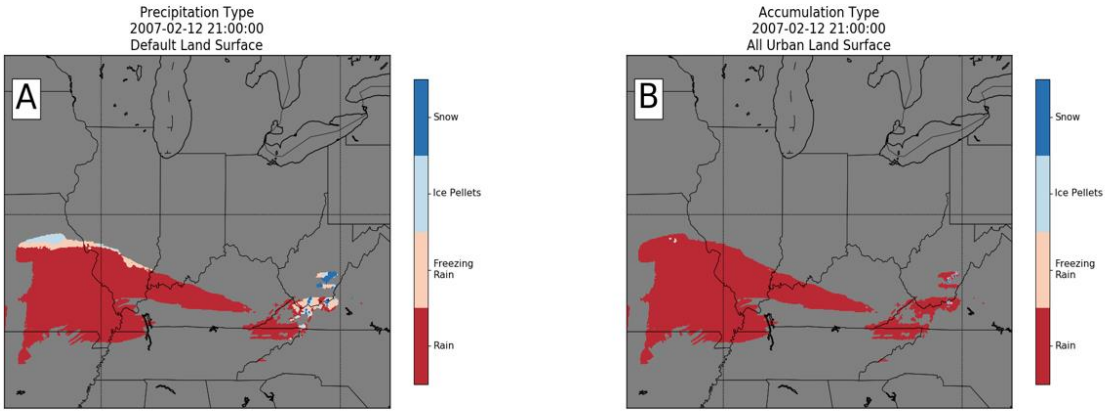

Figure 22A-B: Figure A represents the precipitation-type on the default land surface and acts as the control run for this experiment. Figure B represents the accumulation-type on the all urban land surface. Notice how Figure A shows some frozen precipitation, but the urban land is above freezing, and all hydrometeors would turn to liquid on contact with the surface.

Figure 23 shows the precipitation-type and accumulation-type for February 13 at 09Z. In Figure 23B, there is much more rain accumulation predicted in the southwestern portion of the storm. However, across northeastern Kentucky, RA is predicted to precipitate. The accumulation-type predicted is FZRA due to $T_{skin} < 0°C$. This provides a dangerous hazard to transportation. RA will likely freeze upon contact with a below freezing surface. This occurred in the all urban land surface and not the default land surface run, likely due to the urban land surface cooling faster than the default land surface.

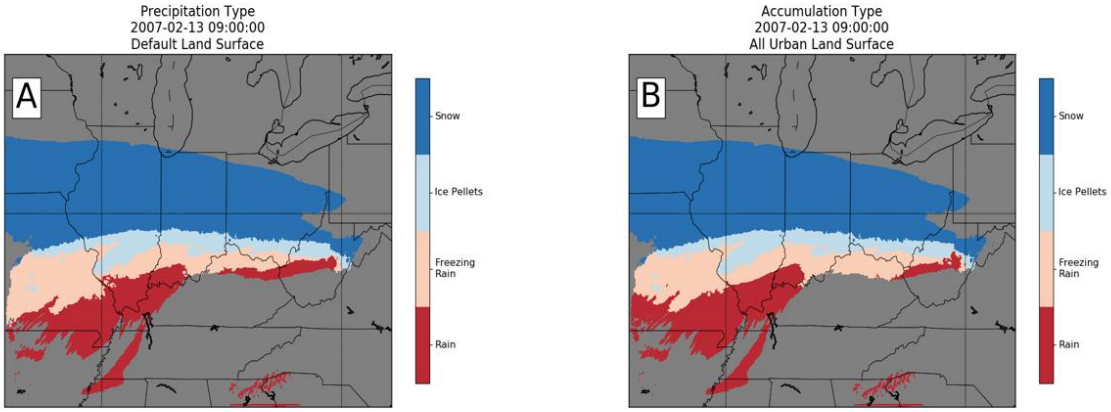

Figure 23A-B: Figure A represents the precipitation-type on the default land surface and acts as the control run for this experiment. Figure B represents the accumulation-type on the all urban land surface. Worth mentioning is the region in northeastern Kentucky where precipitation-type is RA, but accumulation-type is FZRA. This is likely due to the land surface cooling rapidly and the above freezing RA froze on contact with the surface.

Figure 24 shows the precipitation-type and accumulation-type for February 13 at 21Z. The rain line in Figure 24B is much farther northwest than in Figure 24A. This is likely due to the warm temperature and lack of snow cover earlier in the storm over the southwestern portion of the domain.

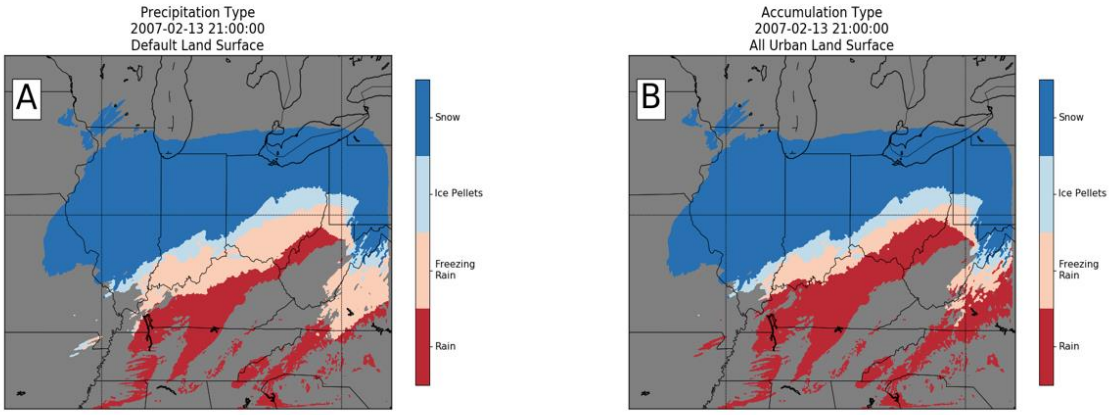

Figure 24A-B: Figure A represents the precipitation-type on the default land surface and acts as the control run for this experiment. Figure B represents the accumulation-type on the all urban land surface. The RA line is pushed northwest as the skin temperature is relatively warm and is not allowing FZRA to accrue on the urban ground.

Figure 25 shows the precipitation-type and accumulation-type for February 14 at 09Z. The accumulation-type algorithm is predicting a robust transition from RA to SN

while the precipitation-type algorithm is predicting a substantial amount of FZRA and IP. The warm urban land surface across southwestern Pennsylvania and into southeastern Kentucky is melting much of the frozen precipitation, similar to Figure 24. The stark contrast is partially due to previous frozen accumulation insulating the urban ground which forces it to stay below freezing. Any area without previous frozen precipitation would not experience the same hindrance.

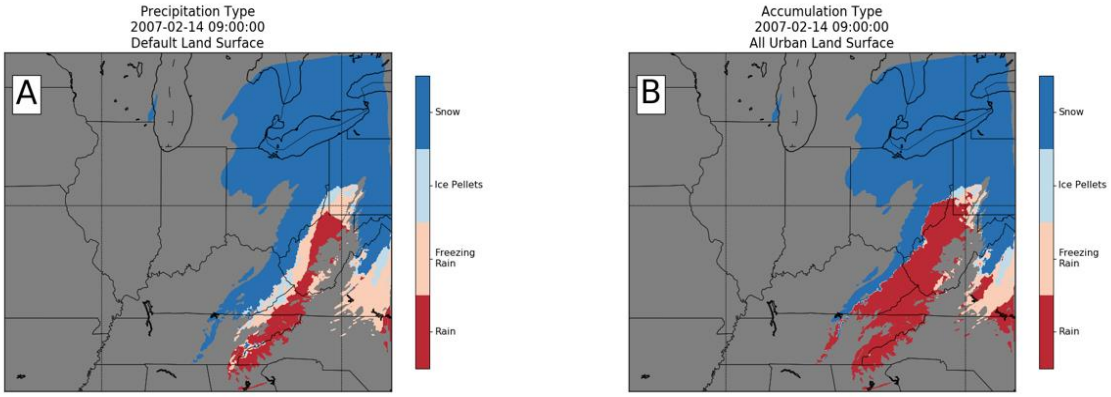

Figure 25A-B: Figure A represents the precipitation-type on the default land surface and acts as the control run for this experiment. Figure B represents the accumulation-type on the all urban land surface. The RA-SN line is well defined with little mixed precipitation. This is likely a consequence of frozen precipitation from earlier in the storm insolating the ground and prohibiting it from heating above freezing. Areas without this catalyst continued to heat above freezing.

Figure 26 shows the precipitation-type and accumulation-type for February 14 at 21Z. The storm has completely transitioned to SN in both Figure 26A and Figure 26B as the northern portion of the domain has been subject to the cold air. All precipitation is falling and accumulating as SN.

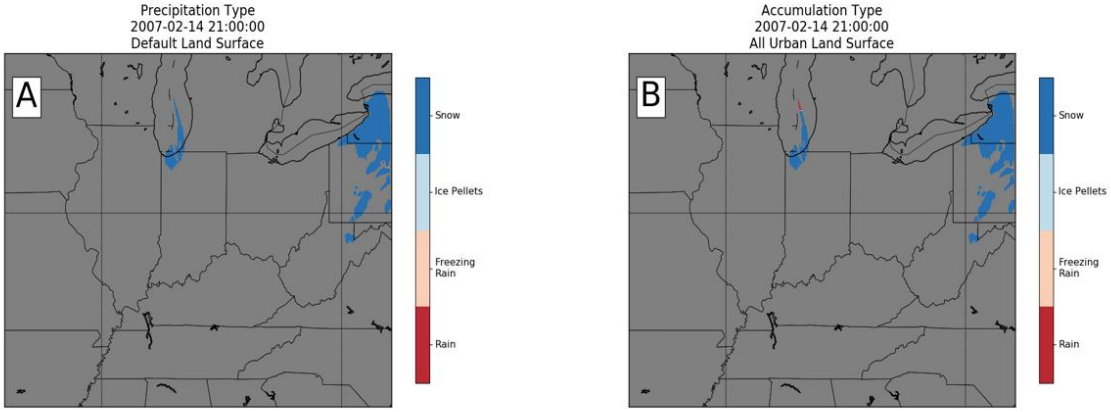

Figure 26A-B: Figure A represents the precipitation-type on the default land surface and acts as the control run for this experiment. Figure B represents the accumulation-type on the all urban land surface. Both figures are showing all snow, meaning that precipitation will not change phase as it encounters the ground.

The alteration of the land surface to all-urban land has drastically influenced what impacts frozen precipitation may accumulate as and how the precipitation may impact transportation. In the majority of figures, the RA line was more robust for the urban parameterization as the skin temperature was typically above freezing in more places than just the locations of RA. In Figure 23A, precipitation is predicted to be RA in northern Kentucky, but accumulation could result in FZRA when RA freezes on contact with the surface. This would lead to a busted forecast and very hazardous driving conditions if Figure 23B were to verify. Areas that began to receive frozen precipitation accumulation during the model run resulted in cooler land surface temperatures and continued to accumulate SN, IP, or FZRA. To the contrary, if an area did not receive frozen precipitation, then there was no inhibitor to prevent the urban land surface from heating above freezing. This led to a stark contrast in the RA-SN line later in the forecast period.

3.4 Experiment 2 Discussion

Experiment 2 analyzed how accumulation-type can vary from precipitation-type when applied to an all urban land surface. The purpose of this experiment was to test how forecasters may better predict the influence winter precipitation could have on transportation. The usefulness of this experiment is provided in the hard-to-forecast region of FZRA and IP. The structure of the region of SN is not altered significantly, and in most cases, the structure of the RA zone grows at the expense of FZRA and IP. In some cases, the ground may heat up during max radiative conditions and exceed freezing, changing the accumulation-type diurnally. However, the most significant difference exists at the beginning of a winter event while the land surface is still too warm.

The urban model's T_{skin} behavior is peculiar at first glance. A strong warm boundary begins to form across the center of the domain. The land surface is reacting to the snow cover and snow cover differs between the urban model and the default model. Regions with no snow cover heat rapidly but a region without snow cover will be insulated and continue to accrue frozen precipitation after initially decreasing below freezing. The urban model's T_{skin} will have a strong diurnal component, increasing rapidly during the day and decreasing in the evening. If T_{skin} decreases enough, SN will begin to accumulate and decrease the diurnal component. SN will sustain itself amidst daytime heating as it is reluctant to melt. In areas that accumulated SN in the default model but not in the urban model, the urban land will continue to heat unbounded during the day, but the default model will maintain a cool, below freezing temperature. Figure 27 shows the snow cover for February 14 at 21z. The very warm temperatures in Figure 21 are

due to the default land surface snow cover and the lack of snow cover in the urban land surface. It is quintessential that forecasters consider the land surface temperature when forecasting winter storms as it may help in distinguishing regions that would have safe driving conditions and regions that would have hazardous driving conditions

Chapter 4: Conclusions

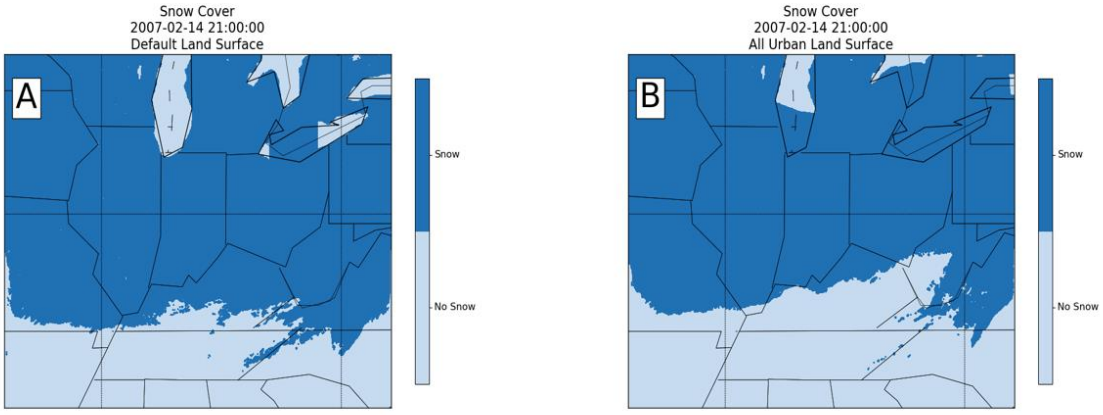

Figure 27A-B: Snow cover at February 14, 21Z. Figure A is default land surface and Figure B is urban land surface. This figure helps to explain the sharp contrast in T_{skin} in Figure 21. The cause of the much warmer urban temperatures is due to the model predicting snow cover in the default land surface but no snow cover in the urban land surface.

4.1 Summary

An accumulation-type algorithm was developed from the algorithms presented by Ramer (1993) and alterations from Pytlak (2010) and Bourgouin (2000) using a decision-tree approach. The Valentine's Day Blizzard of 2007 was chosen as the case study for its robust melting layer. Significant FZRA and IP accumulated from Missouri to Pennsylvania due to the well-defined melting layer. It is not typical that FZRA or IP persist for a multi-day event which makes this storm particularly rare.

The precipitation-type algorithm was used as a control to test the differences in the accumulation-type results. Experiment 1 tested the influence of T_{skin} on the MODIS default land surface during the February 2007 storm. The differences were the greatest

at the beginning of the storm and during the daylight. In the overnight hours, the accumulation-type became nearly identical to the precipitation-type because the ground experienced radiative cooling. The land surface was reluctant to heat back to above freezing where frozen precipitation had accumulated. Overall, the accumulation-type algorithm is particularly useful when a storm begins to impact an area and the precipitation-types and accumulation-types converge.

Experiment 2 analyzed the influence of an all urban land surface on T_{skin} to predict how frozen precipitation may impact transportation. T_w, precipitation, and I_f are derived from the default run to eliminate differences due to the impacts of the land surface alterations on the thermal structure. The accumulation-type on the urban land surface figures differ from the precipitation-type figures due to the lower specific heat of the all urban land surface and it's strong diurnal cycle. In most cases, the RA-zone is more robust due to the warmer T_{skin}. In other cases, such as Figure 23, RA is predicted to be the precipitation, but will likely freeze upon contact with the ground. In Figure 25, the IP and FZRA have withered away and a distinguished like of RA and SN prevails. This is likely because the areas that have already received SN continue to accumulate SN and struggle to heat up above freezing throughout the rest of the storm. By February 14 at 21Z (Figure 26), the storm has converted to all SN and travels to the northeastern CONUS. The accumulation-type algorithm provides a more realistic depiction of what will occur at the surface during a winter storm. Decision-makers should consider what phase a hydrometeor will be as it accrues on the surface and not only what phase the hydrometeor is near the surface.

4.2 Future Work

There is future work that needs to be done to expand upon the testing and development of the accumulation-type algorithm. The first step would be to apply the algorithm to multiple storms and perform verification techniques to determine how useful the algorithm is in practice. Both algorithms would also benefit from allowing hydrometeors to be generated in a layer not-suitable for ice crystal formation as described in Ramer (1993).

Other land surface alterations may cause a more realistic result. A solution is to use a nested domain of an urban land surface and leave the parent domain with a default land surface. Another methodology that may imitate urban areas with adjacent forests or croplands would be a “checker-board” approach; altering every other grid box to urban and leaving the rest of the grid boxes to default could have useful results as well. Expanding upon the accumulation-type algorithm could significantly improve how it performs and how forecasters and decision-makers handle thermodynamically complex winter storms.

References

Baldwin, M., R. Treadon, and S. Contorno, 1994: Precipitation type prediction using a decision tree approach with NMC's mesoscale ETA model. Preprints, *10th Conf. on Numerical Weather Prediction*, Portland, OR, Amer. Meteor. Soc., 30–31.

Black, T. L., 1994: The New NMC Mesoscale Eta Model: Description and Forecast Examples, *Wea. Forecasting*, **9**, 265-278

Bourgouin, P., 2000: A method to determine precipitation type. *Wea. Forecasting*, **15**, 583–592, doi: https://doi.org/10.1175/1520-0434(2000)015<0583:AMTDPT>2.0.CO;2

Changnon, S. A., 2003: Urban modification of freezing-rain events. *J. Appl. Meteor.*, **42**, 863–870, doi: https://doi.org/10.1175/1520-0450(2003)042<0863:UMOFE>2.0.CO;2

Changnon, S. A., and K. E. Kunkel, 2007: Major Winter Storms in the Midwest during Winter 2006-2007. Illinois State Water Survey, 15-22 pp. https://www.ideals.illinois.edu/bitstream/handle/2142/8876/ISWSDCS2007..?sequence=2

Elmore, K. L., H. M. Grams, D. Apps, H. D. Reeves: Verifying Forecast Precipitation Type with mPING. *Wea. Forecasting*, **30**, 656-667, doi: 10.1175/WAF-D-14-00068.1

Heppner, P. O. G., 1992: Snow versus rain: Looking beyond the ‘‘magic’’ numbers. *Wea. Forecasting*, **7**, 683–691. doi: 10.1175/1520-0434(1992)007<0683:SVRLBT>2.0.CO;2

Karlsson, M. 2001: Prediction of hoar-frost by use of a road weather information system. *Meteor. Applications*, **8** 95–105. doi: 10.1017/S1350482701001086

Knollhoff, D. S., E. S. Takle, E. A. Gallus, Jr., D. Burkheimer, 1998: Use of Pavement Temperature Measurements for Winter Maintenance Decisions, *Transportation Conf. Proc.*, 33-36.

Korolev, A., 2007: Limitations of the Wegener-Bergeron-Findeisen Mechanism in the Evolution of Mixed-Phase Clouds, *J. Atmos. Sci.*, **75**, 3372-3375. doi:10.1175/JAS4035.1 (Available online at: http://www.ctre.iastate.edu/pubs/crossroads/33use.pdf)

Lackmann, G. M., K. Keeter, L. G. Lee, and M. B. Ek, 2002: Model representation of freezing and melting precipitation: Implications for winter weather forecasting. *Wea. Forecasting*, **17**, 1016–1033, doi:10.1175/1520-0434(2003)017<1016:MROFAM>2.0.CO;2.

Ladwig, W. (2017). wrf-python (Version 1.1.1). Boulder, Colorado: UCAR/NCAR. doi:10.5065/D6W094P1

Landsberg, H. E. 1981: *The Urban Climate*. Academic Press, 276 pp.

May, R**.** M**.**, Arms, S**.** C**.**, Marsh, P**.**, Bruning, E**. and** Leeman, J**.** R**.**, 2017: MetPy: A Python Package **for** Meteorological Data**,** Unidata, Accessed 31 March 2017. [Available online at https:**//**github**.**com**/**Unidata**/**MetPy**.**] doi:10.5065**/**D6WW7G29**.**

Moyer, B. W., 2000: A climatological analysis of winter precipitation events at Greenville–Spartanburg SC. *Eastern Region Tech*. Attachment 2001-01, Bohemia, NY, 6 pp

Murray, B. J., D. O'Sullivan, J. D. Atkinson, and M. E. Webb, 2012: Ice nucleation by particles immersed in supercooled cloud droplets. *Chem. Soc. Rev*., **41**, 6519-6554, doi:10.1039/c2cs35200a.

Musilek, P., D. Arnold, E. P. Lozowski, 2009: An Ice Accretion Forecasting System (IAFS) for Power Transmission Lines Using Numerical Weather Prediction. *Sci. Online Lett. Atmos.,* **5**, 25-28. doi: 10.2151/sola.2009-007

National Centers for Environmental Prediction/National Weather Service/NOAA/U.S. Department of Commerce, 2000: NCEP FNL Operational Model Global Tropospheric Analyses, continuing from July 1999. Research Data Archive at the National Center for Atmospheric Research, Computational and Information Systems Laboratory, Boulder, CO. [Available online at https://doi.org/10.5065/D6M043C6.] Accessed September 23, 2017.

Pytlak, P., P. Musilek, E. Lozowski, D. Arnold, 2010: Evolutionary Optimization of an Ice Accretion Forecasting System. *Amer. Met. Soc.,* **138**, 2913-2929, doi: 10.1175/2010MWR3130.1

Ramer, J., 1993: An empirical technique for diagnosing precipitation type from model output. Preprints, *Fifth Int. Conf. on Aviation Weather Systems*, Vienna, VA, Amer. Meteor. Soc., 227–230.

Reeves, H. D., K. L. Elmore, A. Ryzhkov, T. Schuur, and J. Krause, 2014: Source of uncertainty in precipitation-type forecasting. *Wea. Forecasting*, **29**, 936–953, doi:10.1175/WAF-D-14-00007.1

Reeves, H. D., A. V. Ryzhkof, and J. Krause, 2016: Discrimination between winter precipitation types based on spectral-bin microphysical modeling. *J. Appl. Meteor. Climatol.,* **55**, 1747–1761, doi:10.1175/JAMC-D-16-0044.1.

Rogers, R. R., M. K. Yau, 1989: *A Short Course in Cloud Physics*. Butterworth-Heinemann, 304 pp.

Sherif, A., Y. Hassan, 2004: Modelling Pavement Temperature for Winter Maintenance Operations, *Can. J. Civ. Eng.* **31**, 369-378, doi: 10.1139/l03-107

Stewart, R. E., and P. King, 1987: Freezing precipitation in winter storms. *Mon. Wea. Rev.*, **115**, 1270–1279, doi:10.1175/1520-0493(1987)115<1270:FPIWS>2.0.CO;2.

Zerr, R. J., 1997: Freezing rain: An observational and theoretical study. *J. Appl. Meteor.*, **36**, 1647–1661, doi:10.1175/1520-0450(1997)036<1647:FRAOAT>2.0.CO;2